Picosecond large angle reorientation of the magnetization in Ni81Fe19 circular thin-film elements

J. Wu, D. S. Schmool, N. D. Hughes, J. R. Moore, and R. J. Hicken

Citation: J. Appl. Phys. **91**, 278 (2002); doi: 10.1063/1.1421211
View online: http://dx.doi.org/10.1063/1.1421211
View Table of Contents: http://jap.aip.org/resource/1/JAPIAU/v91/i1
Published by the American Institute of Physics.

Picosecond large angle reorientation of the magnetization in $Ni_{81}Fe_{19}$ circular thin-film elements

J. Wu,[a] D. S. Schmool,[b] N. D. Hughes, J. R. Moore, and R. J. Hicken[c]
School of Physics, University of Exeter, Stocker Road, Exeter EX4 4QL, United Kingdom

(Received 28 March 2001; accepted for publication 1 October 2001)

Large angle picosecond reorientation of the magnetization has been studied in circular $Ni_{81}Fe_{19}$ thin-film elements of 30 μm diameter and 500 Å thickness by means of an optical pump–probe technique. The sample was pumped by an optically triggered magnetic field pulse and probed by a time resolved magneto-optical Kerr effect measurement. The temporal profile of the pulsed field and the in-plane uniaxial anisotropy of the element were first determined from measurements made in large static fields where the magnetization exhibited small amplitude ferromagnetic resonance oscillations. Measurements of large amplitude oscillations were then made in a smaller static field that was still larger than the in-plane uniaxial anisotropy field and sufficient to saturate the sample. Using the measured temporal profile of the pulsed field, the Landau–Lifshitz–Gilbert equation was used to model the motion of the magnetization as a coherent rotation process. The same values of the anisotropy and damping constants provided an adequate simulation of both the high and low field data. The magnetization was found to move through an angle of up to about 30° on subnanosecond time scales. The dependence of the reorientation upon the direction of the static applied field and observed deviations from the coherent precession model are discussed. © *2002 American Institute of Physics.* [DOI: 10.1063/1.1421211]

I. INTRODUCTION

Fast magnetic reorientation is being intensively studied as higher bit rates are sought in magnetic recording systems. In longitudinal magnetic recording, the alignment of the storage medium has relied upon the thermally activated reversal of an ensemble of single domain particles, while the pole pieces of the write head and the soft layer of the magnetoresistive read sensor have been realigned by a combination of domain wall motion and domain rotation. However, as the switching times of these small magnetic structures move into the picosecond regime, it becomes necessary to rotate all the spins coherently. In this study, we show firstly that the sample anisotropy and the temporal profile of the pulsed field may be characterized by optical pump probe measurements, and secondly, that the same technique may be used to investigate large angle processional motion of the magnetization.

In studies of high speed magnetic reorientation, a magnetic field pulse with a short rise time must be applied to the element under investigation. This may be achieved by discharging a transmission line with a reed switch,[1] the pulse duration being controlled by the length of the transmission line. The sample is placed close to the transmission line and experiences the magnetic field associated with the transient current. Nanosecond pulses of hundreds of kilo-Oersted can be generated in microcoils[2] while kilo-Oersted pulses a few picoseconds in duration can be obtained from the electron beam at a synchrotron source.[3] Much information about the reorientation process may be obtained by examining the remanent state of the sample. However, for a full understanding, it is necessary to observe the full trajectory of the magnetization during the reorientation process. The past decade has seen the development of a number of experimental techniques that allow dynamics to be studied in the time domain with subnanosecond resolution. These include real time inductive[4] and magnetoresistive[5] measurements. With femtosecond pulsed laser sources now commonly available, the optimum temporal resolution has been obtained from magneto-optical pump-probe techniques. The optical pump pulse can be used to trigger a high voltage pulse generator connected to a transmission line, but this technique generally suffers from electronic trigger jitter. This can be eliminated by using a photoconductive switch to directly gate a charged transmission line.[6] Pulsed fields of the order of 1 kOe may be obtained with a bias voltage of the order of 10 V if the width of the transmission line tracks is reduced to just a few microns. Both the linear[7] and nonlinear[8] magneto-optical Kerr effect (MOKE) have been used to probe the magnetization dynamics and information about the motion of the vector magnetization has been obtained.[9–11] The optical technique offers excellent spatial resolution, particularly with the recent development of near field magneto-optical techniques.[12]

The magnetic reorientation process depends firstly upon the strength, shape, and orientation of the field pulse, and secondly upon magnetic and structural properties of the sample such as shape, magnetic anisotropy, the presence of exchange bias fields, and the nature of the magnetic damping. Precessional switching was inferred from experiments in which pulsed fields as small as 2 kOe and of a few picoseconds duration were applied within the plane of a thin mag-

[a]Present address: Department of Physics, University of York, Heslington, York YO10 5DD, United Kingdom.
[b]Present address: Departamento de Fisica, Faculdade de Ciências, Universidade do Porto, R. Campo Alegre 687, P-4169-007 Porto, Portugal.
[c]Electronic mail: r.j.hicken@exeter.ac.uk

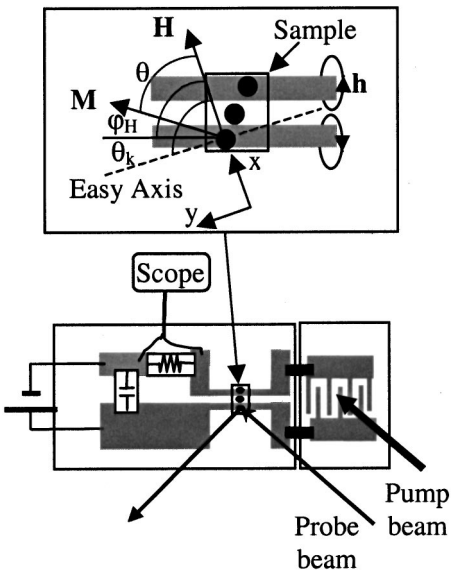

FIG. 1. The measurement geometry and an expanded view of the sample position are shown in schematic form.

netic film.[13] It was found that the pulsed field should be applied orthogonal rather than antiparallel to the initial magnetization direction so as to exert a larger initial torque perpendicular to the film plane. As the magnetization tips out of the film plane, the thin-film demagnetizing field exerts a strong in-plane torque that reduces the switching time. However device applications require fast reorientation of magnetic elements in pulsed fields of more modest strength, and a number of studies have been reported in which time resolved measurements of reorientation have been made after a field pulse has been supplied by a transmission line.[8,11,14] Domain wall processes occur on nanosecond timescales[11] but these may be suppressed by the application of a bias field. Picosecond switching times may then be observed although the switching may still be incoherent. The rise time of the pulsed field within the magnetic element should be as short as possible but may be increased by eddy current shielding[10,15,16] within the element that depends upon the dimensions of the element. The size of the magnetic reorientation is also effected by damping. Ferromagnetic resonance (FMR) experiments made on samples of different thicknesses[17] and on individual samples at different frequencies,[18] have shown that the damping cannot be described by a single phenomenological constant. Simulations suggest that a large amplitude uniform precession decays through the generation of spin waves.[19] Finally, we note that fast switching requires that the magnetization settles quickly into its final orientation. This requires either critical damping of the precessional motion or careful tailoring of the shape of the pulsed field to match the period of precession.[14,20]

It is clear that fast magnetic reorientation is a complicated process and experimental studies are invaluable in advancing our understanding of this phenomenon. In the present work, we study the reorientation of the magnetization in 30 μm diameter $Ni_{81}Fe_{19}$ elements that are expected to exhibit qualitatively similar dynamics to the pole pieces in a thin-film write head structure, or to the free layer in a spin-valve sensor. Our aim has been first to show that all parameters affecting the switching can be deduced from pump–probe measurements. These parameter include the anisotropy constants and damping parameter of the sample, and the temporal profile of the pulsed field. We have then used the pump–probe technique to investigate the reorientation behavior as the relative orientation of a small pulsed field, with a duration of the order of 1 ns, and a static bias field is varied through 360°.

II. EXPERIMENT

The sample chosen for the present study was a circular $Ni_{81}Fe_{19}$ thin-film element of 30 μm diameter and 500 Å thickness produced by a standard photolithographic lift-off technique. A row of identical dots was defined on a glass substrate with a center to center separation of 100 μm chosen to avoid significant dipolar coupling between dots. Photoresist was first spun onto the substrate and patterned, before the $Ni_{81}Fe_{19}$ was sputtered at an Ar pressure of 5 mTorr in a vacuum chamber with a base pressure of 1×10^{-7} Torr. A protective capping layer of 130 Å of Al_2O_3 was deposited without breaking the vacuum. The sputtering was performed in a bias field of 156 Oe produced by a pair of $SmCo_5$ permanent magnets placed in close proximity to the substrate which was at ambient temperature throughout. Finally, the remaining photoresist was removed leaving the row of $Ni_{81}Fe_{19}$ dots.

The basic layout of our optical pump–probe apparatus has been described previously.[9] The experiment is built around a mode-locked Ti:Sapphire laser that produces 100 fs pulses at a repetition rate of 82 MHz. The laser was tuned to a wavelength of 750 nm for the present study. Each pulse is split into a pump and probe component. The pump is used to trigger a current pulse in the device shown in Fig. 1. The device consists of an interdigitated photoconductive switch, grown on a semi-insulating intrinsic GaAs substrate, that is connected to a coplanar stripline. The stripline consists of Au strips of 30 μm width and separation, and is terminated by a 1.5 Ω surface mount resistor and a 47 nF surface mount capacitor before being connected to a 20 V power supply. The temporal profile of the current pulse in the transmission line was monitored with a 500 MHz oscilloscope connected in parallel with the surface mount resistor. The sample was placed face down on the transmission line where it experienced the magnetic field associated with the current. The glass substrate was oriented so that the row of dots made a small angle with the transmission line (this angle has been exaggerated in Fig. 1). This ensured that one dot lay directly above a coplanar strip, and experienced an in-plane pulsed field, while another (not adjacent to the first) lay between the strips and experienced an out-of-plane pulsed field.

A time delay was introduced between the pump and probe pulses by reflecting the pump from a retroreflector on a stepper motor driven translation stage. Both beams were expanded by a factor of 10 and then focused with achromats of 15 cm focal length. The pump spot was defocused to a diameter of about 1 mm on the interdigitated structure. The probe spot was focused to a diameter of less than 20 μm and

was incident upon the back of the glass substrate at an angle of about 43°. The spot positions were monitored continuously with a charge coupled device camera equipped with a zoom lens that gave a ×60 on-screen magnification factor. The probe spot was positioned on the center of the chosen element. Clearly, the large spot size does not allow us to obtain information about the spatial variation of the dynamical magnetization. Measurements were made stroboscopically at a fixed time delay and then the delay was changed to record the magnetic response as a function of the time delay. The probe beam was initially s-polarized and acquired a small rotation and ellipticity due to the MOKE when reflected from the sample. An optical bridge was used to measure the Kerr rotation. By chopping the pump beam and using phase sensitive detection, a resolution of close to 1 μ degree may be achieved. The device shown in Fig. 1 was placed between the pole pieces of an electromagnet so that the transmission line was parallel to the plane of incidence. The electromagnet allowed wide field optical access and could be freely rotated about an axis normal to the sample plane.

III. THEORY

The response of the magnetization of the magnetic element to the pulsed field may be describe by the Landau–Lifshitz–Gilbert equation

$$\frac{\partial \mathbf{M}}{\partial t} = -|\gamma|\mathbf{M}\times\mathbf{H}_{\text{eff}} + \frac{\alpha}{M}\left(\mathbf{M}\times\frac{\partial \mathbf{M}}{\partial t}\right), \tag{1}$$

in which α is the Gilbert damping constant, $\mathbf{H}_{\text{eff}}$ is a total effective field acting upon the magnetization and $\gamma = g\times\pi\times(2.80)$ MHz/Oe where g is the spectroscopic splitting factor. In the most general case, the dynamical magnetization is nonuniform and it is necessary to solve Eq. (1) simultaneously with the Maxwell's equations by means of a finite element analysis. However, we will use a simpler model in which the magnetization of the element is assumed to be uniform and rotates coherently under the influence of the pulsed field. In this case, $\mathbf{H}_{\text{eff}}$ is conveniently evaluated from

$$\mathbf{H}_{\text{eff}} = -\frac{1}{M}\nabla_u E_{\text{tot}} \tag{2}$$

$$E_{\text{tot}} = -\mathbf{M}\cdot[\mathbf{H}+\mathbf{h}(t)] - K_u(\mathbf{u}\cdot\hat{\mathbf{k}})^2 + 2\pi M^2 u_z^2, \tag{3}$$

where $\mathbf{u}=\mathbf{M}/M$ and the total energy density E_{tot} includes the Zeeman energy of the magnetization in the static field $\mathbf{H}$ and the pulsed field $\mathbf{h}(t)$, a uniaxial anisotropy with in-plane easy axis in the direction parallel to the unit vector $\hat{\mathbf{k}}$, and the thin-film demagnetizing energy. For a small amplitude precession of the magnetization, we may derive some simple algebraic results for the precession frequency that we will require later in the analysis of our experimental results. Let us first assume that $|\mathbf{H}|$ is sufficiently large that $\mathbf{h}(t)$ may be neglected when calculating the precession frequency. By minimizing the free energy in Eq. (3), the static orientation of $\mathbf{M}$ is given by

$$MH\sin\theta - K_u\sin[2(\theta_k-\theta)] = 0, \tag{4}$$

where θ_k is the angle between $\mathbf{H}$ and the in-plane easy axis, and θ is the angle between $\mathbf{M}$ and $\mathbf{H}$ as shown in Fig. 1. The precession frequency is then given by

$$\left(\frac{\omega}{\gamma}\right)^2 = \left(H\cos\theta + \frac{2K_u}{M}\cos[2(\theta_k-\theta)]\right) \times\left(H\cos\theta + \frac{2K_u}{M}\cos^2(\theta_k-\theta) + 4\pi M\right). \tag{5}$$

Let us now retain $\mathbf{h}(t)$ but instead assume that $\mathbf{M}$ is quasi-aligned with $\mathbf{H}' = \mathbf{H}+\mathbf{h}(t)$. In this case, the precession frequency is given by

$$\left(\frac{\omega}{\gamma}\right)^2 = \left(H' + \frac{2K_u}{M}\cos 2\theta_k\right)\left(H' + \frac{2K_u}{M}\cos^2\theta_k + 4\pi M\right) \tag{6}$$

$$H' = (H^2\cos^2\varphi_H + (H\sin\varphi_H - h)^2)^{1/2}, \tag{7}$$

where φ_H is the angle between $\mathbf{H}$ and the optical plane of incidence as shown in Fig. 1. When the amplitude of precession is not small then Eq. (1) may be solved numerically if the temporal profile of the pulsed field is known. Since the element is thicker than the optical skin depth, generalized Fresnel reflection coefficients for the interface between a dielectric and ferromagnetic metal may be used to calculate the instantaneous Kerr rotation of the probe beam due to a mixture of the longitudinal and polar Kerr effects as we have discussed previously.[15]

IV. CHARACTERIZATION OF THE PULSED FIELD

It is essential to determine the temporal profile of the pulsed magnetic field before attempting to interpret the results of the pump–probe experiments. The trace obtained from the oscilloscope, which has been plotted in Figs. 2(a) and 2(b), gives a general impression of the pulse shape that is useful when aligning the pump beam. The trace shows oscillations with a period of the order of 1 ns that are associated with reflections of the pulse from the power supply. However, the trace does not reveal the finer features of the pulse shape due to the finite bandwidth (500 MHz) of the oscilloscope. Also, the height of the trace is not a reliable measure of the current amplitude because the small value surface mount resistor has considerable inductive impedance at high frequencies[21] that is difficult to characterize. In order to estimate the amplitude of the current, we instead attached the oscilloscope across the interdigitated switch and measured the drop in voltage that occurs when the switch is gated. Taking into account the bandwidth of the oscilloscope, we estimate a peak voltage change of about 30% of the bias voltage. We calculate[22] that our transmission line has a characteristic impedance of approximately 86 Ω, which implies a peak current of 70 mA in the transmission line. By integration of the Biot–Savart law we calculate a peak pulsed field of about 15 Oe immediately above the tracks of the transmission line.

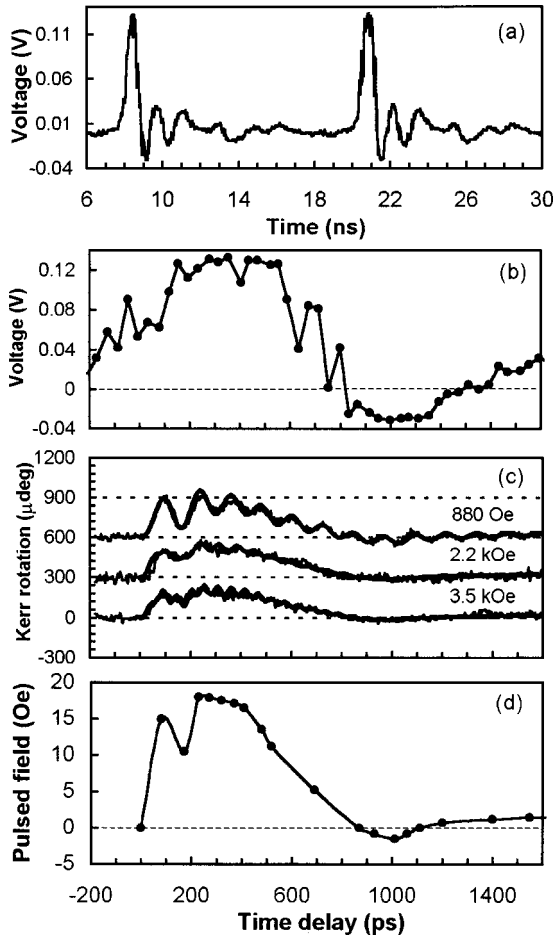

FIG. 2. (a) and (b) The pulse shape obtained from the oscilloscope is shown on two different time scales. (c) Measured (fine line) and simulated (bold line) high field FMR oscillations are shown. (d) The pulsed field profile used to produce the simulations in (c) is shown.

High field FMR measurements can be used as a high bandwidth probe of the temporal profile of pulsed magnetic fields.[23] When FMR oscillations are induced by a pulsed field applied in the plane of a thin-film sample, the large thin-film demagnetizing field causes the magnetization to be highly elliptical with the long axis of the ellipse lying in the sample plane. However, if the pulsed field is applied perpendicular to the film plane, then the trajectory has a more circular shape.[9,16] In this case, the measured Kerr rotation is dominated by the polar MOKE signal from the out-of-plane component of the dynamical magnetization. The shape of the envelope of the oscillatory Kerr signal then follows the temporal profile of the pulsed field and is relatively insensitive to the values of the optical constants of the sample. With this in mind, the probe beam was focused on the element between the tracks of the transmission line, where the pulsed field lies perpendicular to the plane of the sample, and relatively large static fields were applied in the plane of the sample and perpendicular to the plane of incidence. The Kerr rotations recorded for three different static field values are shown in Fig. 2(c). The flat trace at negative time delays suggests that resonant pumping from successive laser pulses can be ignored.

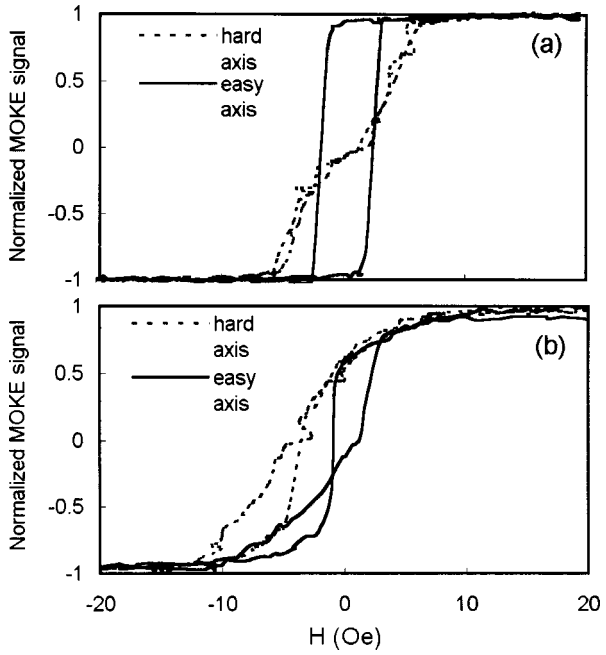

FIG. 3. (a) Hard and easy axis loops are plotted for the continuous $Ni_{81}Fe_{19}$ film. (b) Hard and easy axis loops are plotted for the circular $Ni_{81}Fe_{19}$ thin-film element.

Simulations were performed by solving the Landau–Lifshitz–Gilbert equation numerically and calculating the expected Kerr rotation. The oscilloscope trace was used as a first guess of the true pump field profile. The simulations are insensitive to the in-plane anisotropy field due to the large value of the static field, but the values of the spontaneous magnetization M, the g factor, and the damping constant α must be adjusted to reproduce the shape of the oscillations. The simulations for the three static field values were compared with the experimental traces and the pump field profile was gradually adjusted until the simulations were in satisfactory agreement with the data. The final profile, shown in Fig. 2(d), is qualitatively similar to the original oscilloscope trace but the rise time is now much shorter and there is evidence of short time scale reflections that arise from impedance mismatches on the transmission line structure itself. This temporal profile was used in all subsequent calculations. Finally, we note that provisional values of the sample parameters are sufficient for the initial characterization of the pulsed field. These will be discussed again in the next section where the final values are determined more accurately. The final values for M, K_u, and g have been used in the simulations of Fig. 2(c) to ensure self-consistency in the fitting, but a somewhat larger value of $\alpha = 0.02$ was required, which we will discuss in the final section of this article.

V. SAMPLE CHARACTERIZATION

The in-plane anisotropy of the sample was initially studied by longitudinal MOKE measurements at a wavelength of 633 nm with a focused spot size of about 20 μm. Hysteresis loops were acquired by probing through the glass substrate with the magnetic field applied at various angles in the plane of the sample. Measurements were first made with an unfo-

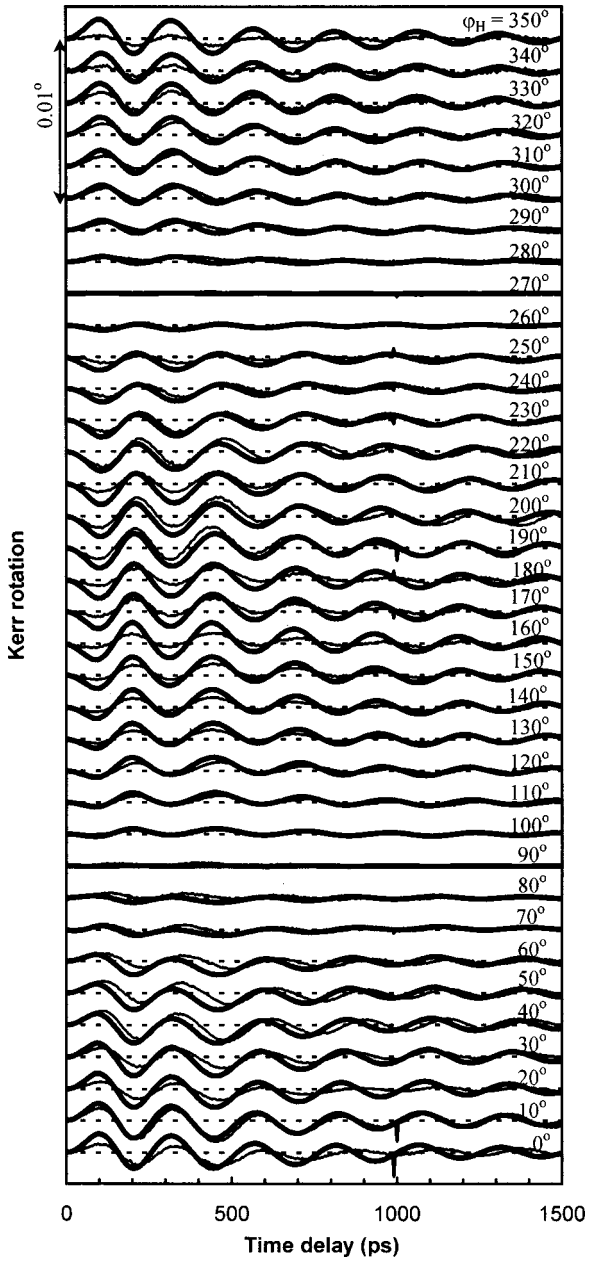

FIG. 4. Time dependent Kerr rotation is plotted for measurements in which a static field of 216 Oe was applied in different directions in the sample plane. The fine and bold curves represent the measured and simulated rotation, respectively.

cused beam on a continuous film of similar thickness. The results are shown in Fig. 3(a) and reveal a clear uniaxial character and a hard axis saturation field of about 7 Oe. The easy axis direction corresponds to that of the magnetic field applied during the film growth. The loops obtained from the circular element were more distorted, suggesting that the signal obtained with the focused laser spot is an ill-defined average from a few domains within the element. The domain structure may also be different to that in the continuous films due to the modified dipolar energy and the introduction of additional pinning sites at the edge of the element. In Fig. 3(b), we show loops corresponding to the hard and easy directions as determined from pump–probe measurements that we discuss in the next paragraph. Clearly, the anisotropy field cannot be easily determined from these hysteresis loops.

Pump–probe measurements were next made on the element centered on the lower track of the transmission line where the pulsed field lay in the sample plane, pointing vertically downward as shown in Fig. 1. A static field of 216 Oe was applied in different directions in the plane of the sample. Measurements were made as the field was rotated through 360° in steps of 10°. The measured Kerr rotation has been plotted in Fig. 4. The static field is sufficiently large that the magnetization is quasi-aligned with the static field. We see that the amplitude of the Kerr signal is a minimum when the pulsed and static fields are parallel. This is easily understood since the pulsed field exerts no torque upon the magnetization in this case. Fast Fourier transforms were taken of the experimental data. The power spectra showed single peaks whose positions have been plotted in Fig. 5. Although there is some scatter in these measured frequencies, it is immediately obvious that the frequencies do not have the 180° period expected for a sample with uniaxial anisotropy. The symmetry is reduced by the presence of the pulsed field which remains fixed as the static field is rotated and which has magnitude of similar order to that of the in-plane anisotropy field. Equations (6) and (7) may be used to describe this variation if some further approximations are made to account for the time dependence of the pulsed field. First, we assume that the effective static orientation of $\mathbf{M}$ is parallel to $\mathbf{H}$ rather than the instantaneous total field $\mathbf{H}'=\mathbf{H}+\mathbf{h}(t)$. Secondly, since the magnitude of the pulsed field is time dependent, we use an average value of 6.8 Oe determined from Fig. 2. Assuming also a value of $g=2$, Eqs. (6) and (7) were fitted to the measured frequency values. The fit yielded values of $M=720$ emu/cm^3 and $2K_u/M=12$ Oe. The orientation of the easy axis was found to be 20° from the optical plane of incidence and hence also 20° from the direction of the magnetic field applied during the film growth. These parameters values and a damping constant of $\alpha=0.012$ were then used in all subsequent calculations. Simulated Kerr rotation traces have been plotted in Fig. 4 and are in reasonable qualitative agreement with the experimental data. We do not expect to reproduce the amplitude of oscillation correctly because the optical constants of the film are not sufficiently well known, indeed, we use values reported for pure nickel.[16] The complex optical constants influence the way in which the longitudinal and polar Kerr effects combine to give the total rotation signal. The longitudinal and polar contributions change with field azimuth due to changes in both the trajectory of the magnetization precession and the optical geometry. An incorrect choice of optical constants can lead to some variation in the relative amplitudes of the simulations and experimental data for different azimuths in Fig. 4. Frequencies obtained from Fourier transforms of the simulations have also been plotted in Fig. 5 and lie close to the curve calculated from Eqs. (4) and (7). The good agreement between experiment and simulation in Fig. 5 gives additional credence to the pulsed field values shown in Fig. 2.

Measurements were next made as a function of the static field strength with the static field applied in the plane of incidence at an angle of $\varphi_H=180°$. The results are shown in

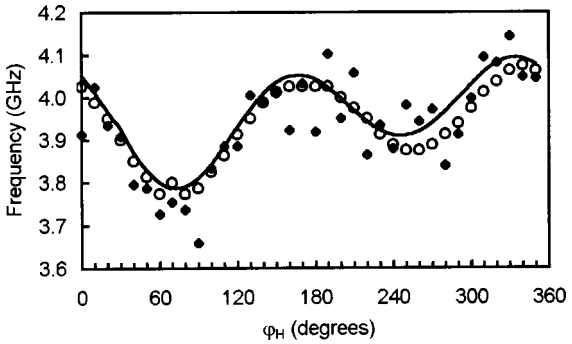

FIG. 5. The frequencies of oscillation of the curves in Fig. 4 are plotted as a function of φ_H. The frequencies of the measured and simulated curves are represented by diamond and circular symbols, respectively. The curve was calculated from Eqs. (6) and (7).

Fig. 6(a). Simulated curves are also shown that are in good qualitative agreement with the experimental data. In each case, the equilibrium orientation of the static magnetization was calculated from Eq. (4) and used as the starting point for the time dependent calculation. The frequencies of oscillation of the measured curves were again determined from the Fourier power spectra and are plotted in Fig. 6(b) with a curve calculated from Eqs. (4) and (5). The parameter values assumed in Fig. 5 were used again in Fig. 6(b), and their validity is confirmed by the good agreement between the curve and the measured frequencies.

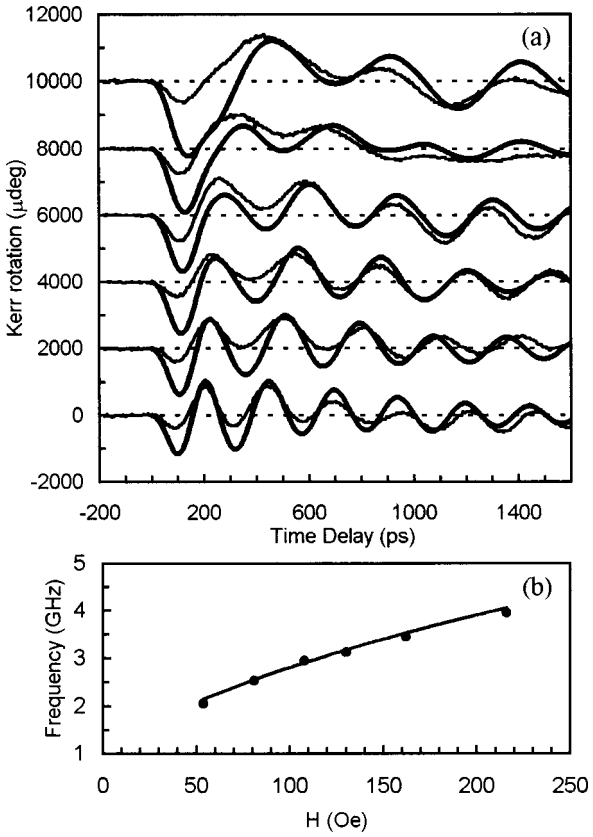

FIG. 6. (a) The measured (fine line) and simulated (bold line) Kerr rotation is plotted for different values of the static field for the case that $\varphi_H = 180°$. (b) The FMR frequencies deduced from the experimental curves in (a) are plotted against the value of the static field. The curve was calculated from Eqs. (4) and (5).

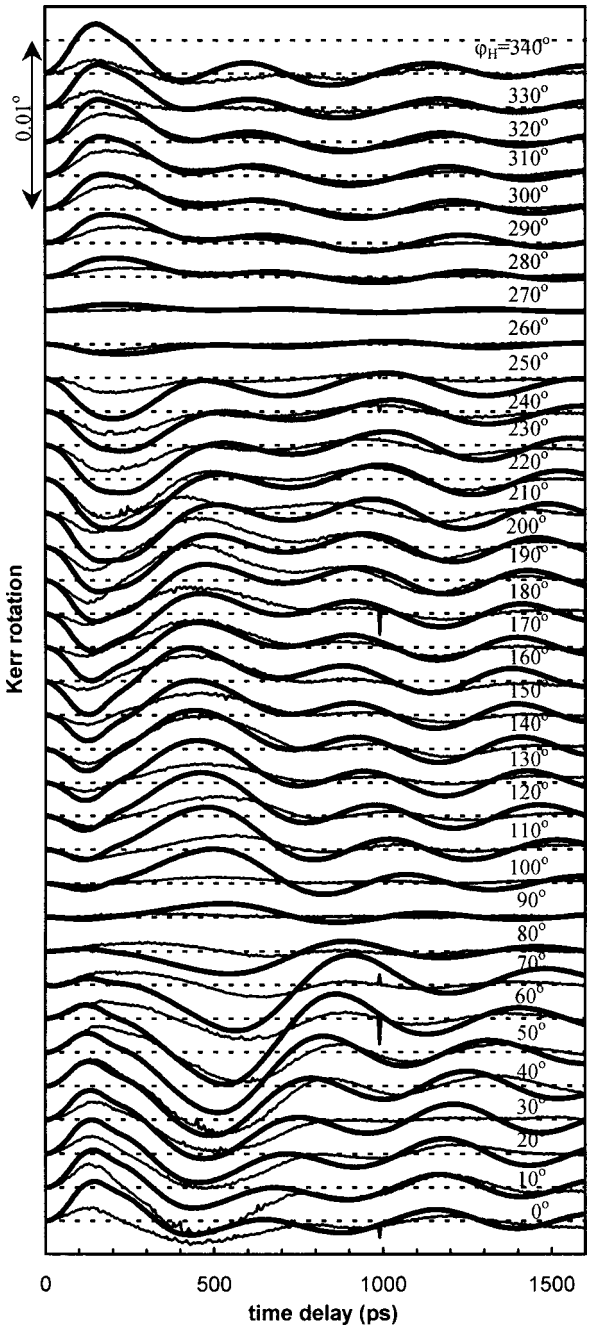

FIG. 7. Time dependent Kerr rotation is plotted for measurements in which a static field of 54 Oe was applied in different directions in the sample plane. The fine and bold curves represent the measured and simulated rotation, respectively.

VI. MEASUREMENTS OF LARGE ANGLE REORIENTATION

Having characterized the pulsed field and the magnetic properties of the $Ni_{81}Fe_{19}$ dot immediately above the lower track of the transmission line, the rotation scan of Fig. 4 was repeated in a smaller static field of 54 Oe. The measured and simulated Kerr rotations have been plotted in Fig. 7. The general trends are the same in the two sets of curves in Fig.

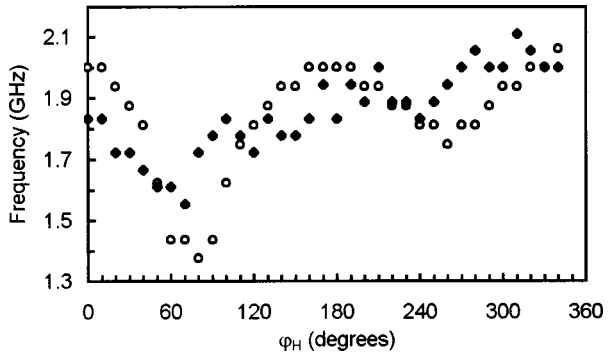

FIG. 8. The frequencies of oscillation of the curves in Fig. 8 are plotted as a function of φ_H. The diamond and circle symbols correspond to the experimental and simulated curves, respectively.

7 but the agreement between experiment and simulation is generally poorer than in Fig. 4. Fourier transforms were again taken of both the experimental and simulated Kerr rotation curves and the peak frequencies are plotted in Fig. 8. The frequencies of the simulated curves are seen to vary through a greater range than those of the experimental curves. However, it is debatable whether the Fourier transform of so few periods of oscillation is really a reliable measure of the average precession frequency. No curve appears in Fig. 8 because Eqs. (6) and (7) are no longer valid in the low field limit.

If we assume that the simulations do provide an adequate description of the dynamics, then we may consider the trajectory of the magnetization corresponding to each trace in Fig. 7. As we mentioned previously, the magnetization exhibits a very flat precession ($M_z \ll M$) due to the influence of the thin-film demagnetizing field and the fact that the pulsed field lies in the plane of the sample. We define the in-plane reorientation angle φ_R as the maximum angular deviation of the projection of the magnetization upon the $x-y$ plane. The dependence of φ_R upon φ_H has been plotted in Fig. 9(a). The scatter in the graph results from the form of $\mathbf{h}(t)$ used in the simulation. The motion is sensitive to the relative phase of the peaks in $\mathbf{h}(t)$ and the precession of the magnetization,[14,20] and this varies in a complicated way as the orientation of the static field is changed. As expected the magnitude of φ_R is a minimum when φ_H is close to 90° and 270° because **M** and $\mathbf{h}(t)$ are almost parallel and so little torque is applied to **M**. The Kerr rotation and the time dependence of the magnetization have been plotted in Figs. 9(b) and 9(c), respectively, for the $\varphi_H = 40°$ azimuth (**H** and **h** are 130° apart) which lies close to the maximum in the φ_R curve. From Fig. 7, it can also be seen that the simulated and experimental Kerr rotations agree particularly well for this azimuth. Figure 9(c) suggests that a reorientation angle of close to 30° occurs about 350 ps after the application of the pulsed field.

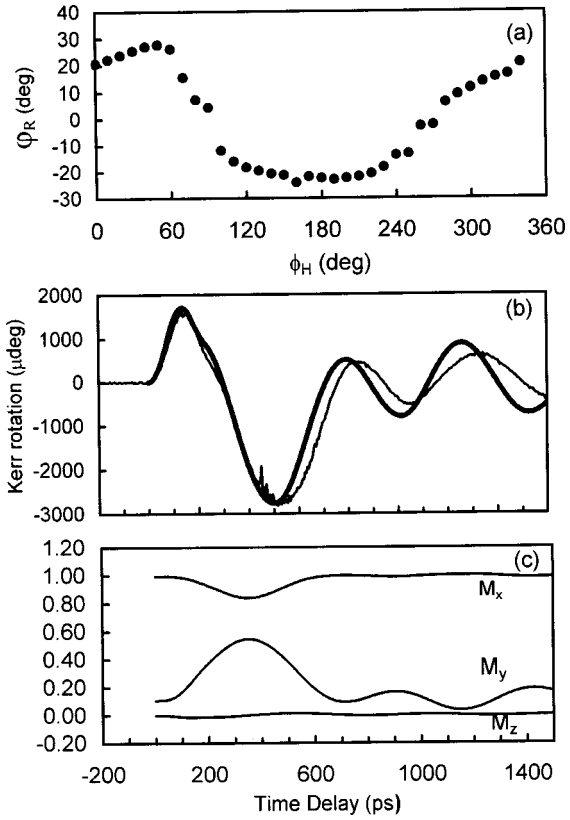

FIG. 9. (a) The maximum angular deviation of the projection of the magnetization upon the $x-y$ plane, φ_R, is plotted against the angle φ_H defined in Fig. 1. (b) The experimental (fine line) and simulated (bold line) Kerr rotations are plotted for $\varphi_H = 40°$. (c) The three components of the magnetization are plotted as a function of time for the $\varphi_H = 40°$ simulation.

VII. DISCUSSION

The results presented in the preceding sections demonstrate the utility of the optical pump–probe technique both for the investigation of picosecond magnetic processes and the characterization of basic material properties. High field measurements can probe the pulsed field profile with a bandwidth limited by the FMR frequency that is in turn limited by the magnitude of the static field that may be applied. A bandwidth of about 20 GHz was adequate for the present study since the aim was to characterize the pulse used in measurements at much lower static fields. Since the precession frequency is only about 2 GHz in these latter measurements, the motion of the magnetization is relatively insensitive to Fourier components of the pulsed field with frequency greater than 20 GHz. We expect the pulsed field within the sample to rise more slowly when the pulsed field is applied perpendicular rather than parallel to the sample plane due to eddy current shielding.[15,16] The rise time of the pulse used in the low field reorientation measurements may be some tens of picoseconds shorter than that determined in Sec. IV. This may affect the phase of the oscillations shown in Figs. 4 and 7, but, due to the complicated shape of the pulse profile, we have not attempted to account for this effect. We would expect the out-of-plane component of the magnetization M_Z to generate eddy currents at the circumference of the circular element. We have already noted that the precession trajectory has a more circular shape and hence a larger M_z component when the pulsed field is perpendicular to the sample plane. This may explain why a larger damping constant was required in the characterization of the pulsed field.

The in-plane magnetic anisotropy of the $Ni_{81}Fe_{19}$ element could not be easily determined from the MOKE hys-

teresis loops because the detailed quasi-static micromagnetic reversal process was not known. MOKE microscopy would provide more information but domain images generally require further interpretation before the anisotropy strength can be deduced. Pump–probe measurements of the frequency of precession in a large static applied field are more reliable because the sample is always saturated. We note that hysteresis loops from continuous films grown simultaneously with the dots may be misleading. We suggest that the photolithographic lift-off technique may lead to strain relief in the circular element that affects a change in the magnetic anisotropy. This might explain the observation that the uniaxial anisotropy axis was misaligned from the direction of the magnetic field applied during the sample growth. More detailed structural studies are required to confirm this suggestion. The inclusion of the average pulsed field in Eqs. (6) and (7) for the precession frequency is a simple but crude approximation. In reality, the instantaneous precession frequency changes continuously as the magnitude of the pulsed field changes. However, we have demonstrated that this approach provides a useful check on the calculated pulsed field strength in the present case and we expect that the pulsed field strength could be determined more accurately for fields with simpler temporal profiles such as the step fields that we have used previously.[9]

We have assumed that the pulsed field is uniform across the area of the circular element and that its value is equal to that calculated at the center of the element. In fact, there is some variation in the magnitude and direction of the pulsed field across the width of the coplanar stiplines as we have discussed previously.[16] Nevertheless, the coherent rotation model appears to work well for large static fields and good qualitative agreement is obtained between experiment and simulation in Fig. 4. While better agreement could be obtained through further variation of the sample parameters for each azimuth, our aim has been to be obtain the best overall agreement with a single set of parameters. Adjustment of the optical constants might further improve the simulations but we have not attempted to do this due to the computation time required. We also note that any misalignment of the s-polarized beam gives rise to a small p-polarized component, the intensity of which may change due to the transverse Kerr effect, leading to an effective rotation of the total electric field. We would expect this effect to be most obvious around $\varphi_H = 0$ and 180° in Fig. 4 where there is a large time dependent component of the magnetization transverse to the plane of incidence. Since the agreement between experiment and simulation is no worse for these azimuths than for others in Fig. 4, we conclude that this misalignment effect is probably not significant in the present study.

We expect the magnetization to reorient by a rotation process, even in the smaller static field used in Fig. 7, because the sum of the static and pulsed fields $\mathbf{H}'$ is always larger than the anisotropy field. The static field is essential for our stroboscopic measurement technique since it returns the system to its initial state after each pulse has been applied. However, this case is also of technological interest since a bias field may be built into a thin-film structure by means of interlayer exchange coupling to a high coercivity underlayer or by direct exchange coupling to an antiferromagnet. The disagreement between simulation and experiment for some values of φ_H may indicate that the rotation process is becoming incoherent. The good agreement between experiment and simulation in Fig. 9(b) suggests that the magnetization can be switched through an angle of up to 30° by means of a rotation process. The maximum switching angle occurred when $\varphi_H = 50°$ so that $\mathbf{h}$ and $\mathbf{H}$ were 140° apart. An angle of 90° is expected to be best for very short pulsed fields since then the maximum torque is applied to the magnetization before it reorients significantly. In the present case, the pulsed field has longer duration and a somewhat different orientation of the pulsed field is required so that the maximum integrated torque is obtained during the reorientation process. The damping constant α was found to be similar for both the small and large amplitude motion of Figs. 4 and 7, suggesting that the uniform precession is not strongly damped by spin wave generation under the present conditions. In future studies, it would be interesting to explore how well the coherent model applies and whether the value of the damping parameter remains unchanged as the value of the static field is reduced further.

In conclusion, optical pump–probe experiments have shown that reorientation through angles of up to 30° may be achieved in times as short as 350 ps in $Ni_{81}Fe_{19}$ thin-film elements. The motion is well described by a coherent rotation process. However, to understand this behavior, it is necessary to perform a thorough characterization of the magnetic properties of the element and determine the temporal profile of the pulsed magnetic field. We have shown how this may be achieved with pump–probe measurements made in larger static applied fields on the same sample. Larger pulsed magnetic field are now required to extend these measurements to a wider range of magnetic materials and improved spatial resolution is required so that the coherence of the switching may be explored in greater detail.

ACKNOWLEDGMENT

The authors gratefully acknowledge the financial support of the United Kingdom Engineering and Physical Sciences Research Council (EPSRC).

[1] R. P. Cowburn, J. Ferré, S. J. Gray, and J. A. C. Bland, Phys. Rev. B **58**, 11507 (1998).
[2] K. Mackay, M. Bonfim, D. Givord, and A. Fontaine, J. Appl. Phys. **87**, 1996 (2000).
[3] C. H. Back, D. Weller, J. Heidmann, D. Mauri, D. Guarisco, E. L. Garwin, and H. C. Siegmann, Phys. Rev. Lett. **81**, 3251 (1998).
[4] T. J. Silva, C. S. Lee, T. M. Crawford, and C. T. Rogers, J. Appl. Phys. **85**, 7849 (1999).
[5] R. H. Koch, J. G. Deak, D. W. Abraham, P. L. Trouilloud, R. A. Altman, Y. Lu, W. J. Gallagher, R. E. Scheuerlein, K. P. Roche, and S. S. P. Parkin, Phys. Rev. Lett. **81**, 4512 (1998).
[6] M. R. Freeman, R. R. Ruf, and R. J. Gambino, IEEE Trans. Magn. **27**, 4840 (1991).
[7] W. K. Hiebert, A. Stankiewicz, and M. R. Freeman, Phys. Rev. Lett. **79**, 1134 (1997).
[8] T. M. Crawford, T. J. Silva, C. W. Teplin, and C. T. Rogers, Appl. Phys. Lett. **74**, 3386 (1999).
[9] R. J. Hicken and J. Wu, J. Appl. Phys. **85**, 4580 (1999).
[10] Y. Acreman, C. H. Back, M. Buess, O. Portmann, A. Vaterlaus, D. Pescia, and H. Melchior, Science **290**, 492 (2000).

[11] B. C. Choi, M. Belov, W. K. Hiebert, G. E. Ballentine, and M. R. Freeman, Phys. Rev. Lett. **86**, 728 (2001).
[12] M. R. Freeman, A. Y. Elezzabi, and J. A. H. Stotz, J. Appl. Phys. **81**, 4516 (1997).
[13] C. H. Back, R. Allenspach, W. Weber, S. S. P. Parkin, D. Weller, E. L. Garwin, and H. C. Siegmann, Science **285**, 864 (1999).
[14] M. Bauer, R. Lopusnik, J. Fassbender, and B. Hillebrands, Appl. Phys. Lett. **76**, 2758 (2000).
[15] J. Wu, J. R. Moore, and R. J. Hicken, J. Magn. Magn. Mater. **222**, 189 (2000).
[16] J. Wu, N. D. Hughes, J. R. Moore, and R. J. Hicken, J. Magn. Magn. Mater. (in press).
[17] A. Azevedo, A. B. Oliveira, F. M. de Aguiar, and S. M. Rezende, Phys. Rev. B **62**, 5331 (2000).
[18] J. F. Cochran, R. W. Qiao, and B. Heinrich, Phys. Rev. B **39**, 4399 (1989).
[19] E. D. Boerner, H. N. Bertram, and H. Suhl, J. Appl. Phys. **87**, 5389 (2000).
[20] T. M. Crawford, P. Kabos, and T. J. Silva, Appl. Phys. Lett. **76**, 2113 (2000).
[21] Philips Components Application Note, ''Space-saving 4-resistor arrays in 0804 package.''
[22] K. C. Gupta, R. Garg, and I. J. Bahl, *Microstrip Lines and Slotlines* (Artech House, Boston, 1979).
[23] A. Y. Elezzabi and M. R. Freeman, Appl. Phys. Lett. **68**, 3546 (1996).